Evidence for supercurrent connectivity in conglomerate particles in $NdFeAsO_{1-\delta}$

2008 Supercond. Sci. Technol. 21 092004

(http://iopscience.iop.org/0953-2048/21/9/092004)

Supercond. Sci. Technol. **21** (2008) 092004 (5pp) doi:10.1088/0953-2048/21/9/092004

RAPID COMMUNICATION

Evidence for supercurrent connectivity in conglomerate particles in $NdFeAsO_{1-\delta}$

J D Moore[1], K Morrison[1], K A Yates[1], A D Caplin[1], Y Yeshurun[1,4], L F Cohen[1], J M Perkins[2], C M McGilvery[2], D W McComb[2], Z A Ren[3], J Yang[3], W Lu[3], X L Dong[3] and Z X Zhao[3]

[1] Blackett Laboratory, Imperial College, London SW7 2AZ, UK
[2] Materials Department, Imperial College, London SW7 2AZ, UK
[3] National Laboratory for Superconductivity, Institute of Physics and Beijing National Laboratory for Condensed Matter Physics, Chinese Academy of Sciences, PO Box 603, Beijing 100190, People's Republic of China

Received 3 June 2008, in final form 19 June 2008
Published 4 July 2008
Online at stacks.iop.org/SUST/21/092004

Abstract
Here we report the use of global and local magnetometry and Hall probe imaging to investigate the electromagnetic connectivity of the superconducting current path in the oxygen-deficient fluorine-free Nd-based oxypnictides. High resolution transmission electron microscopy and scanning electron microscopy show strongly layered crystallites, evidence for a ∼5 nm amorphous oxide around individual particles, and second phase neodymium oxide which may contribute to the large paramagnetic background at high field and at high temperatures. From global magnetometry and electrical transport measurements it is clear that there is a small supercurrent flowing on macroscopic sample dimensions (mm), with a lower bound for the average (over this length scale) critical current density of the order of 10^3 A cm^{-2}. From magnetometry of powder samples and local Hall probe imaging of a single large conglomerate particle ∼120 μm it is clear that, on smaller scales, there is better current connectivity with a critical current density of the order of 5×10^4 A cm^{-2}. We find enhanced flux creep around the second peak anomaly in the magnetization curve and an irreversibility line significantly below $H_{c2}(T)$ as determined by ac calorimetry.

(Some figures in this article are in colour only in the electronic version)

1. Introduction

The generic composition of the quaternary oxypnictides is LPMPn (L = La, Pr, Ce, Sm); M = Mn, Fe, Co, Ni; Pn = P, As. The crystal structure of the parent compound LaFeAsO is well established, and the band structure, the multi-sheet Fermi surface of the doped (superconducting) compound, the density of states, and the electron–phonon coupling have all been calculated theoretically [1–5]. These are layered materials (and hence significantly anisotropic) in which in the undoped parent compound the (conducting) Fe_2As_2 layer is sandwiched between (insulating) La_2O_2 layers. Doping the La_2O_2 layer by replacing the O^{2-} with F^- provides extra positive charge in the insulating layer and negative charge in the conduction layer. The material is then a low carrier density semi-metal but with a high density of states near the Fermi energy (because of a van Hove singularity), and is on the verge of itinerant magnetism [2]. There is no theoretical consensus yet concerning the symmetry of the order parameter [3, 6, 7] nor whether the multiple sheets of the Fermi surface manifest themselves as a multi-gap superconductor. For the $LaFeAsO_{1-x}F_x$ compound, strong electron–electron correlations are suggested from the temperature-dependent resistivity, Seebeck coefficient, and thermal conductivity data [8]. Combined neutron scattering data, specific heat measurements, and Hall data show that

[4] Permanent address: Institute of Superconductivity, Department of Physics, Bar-Ilan University, Ramat-Gan, 52900, Israel.

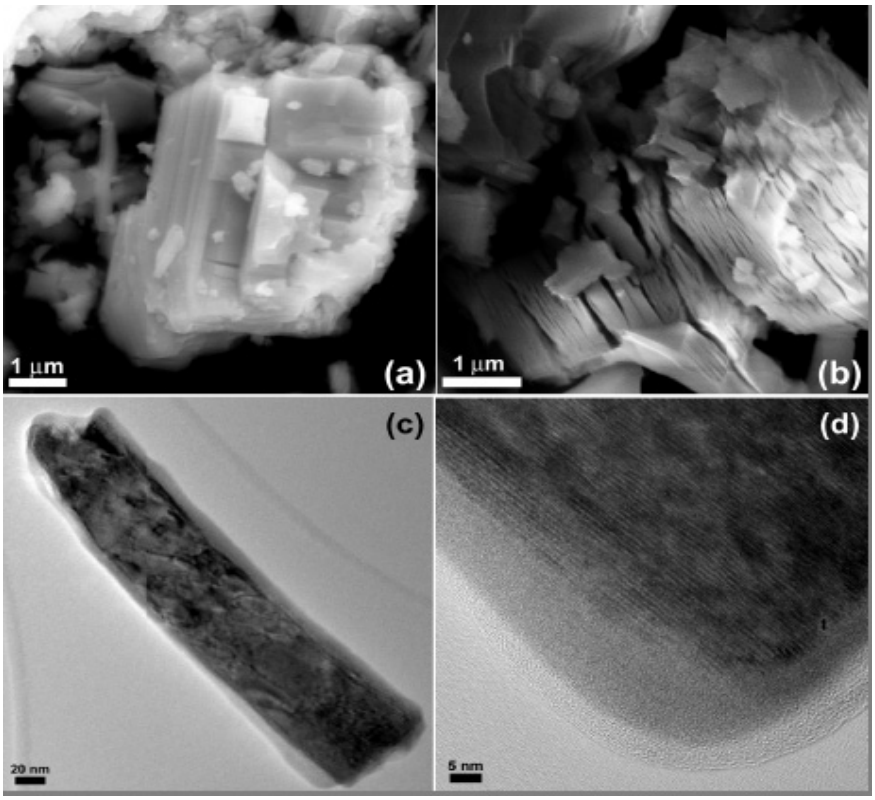

Figure 1. (a) FE-SEM image of a typical $NdFeAsO_{1-\delta}$ particle from the as-sintered body. (b) Neodymium oxide particle; chemistry confirmed using EDX from various positions on the particle. This grain shows a different morphology to the more platelet-like superconducting grains. Furthermore, the fracture paths of the platelet $NdFeAsO_{1-\delta}$ grains show a possible layered structure. (c) and (d) Low and high magnification TEM images of a single $NdFeAsO_{1-\delta}$ grain showing both evidence of a layered structure as well as an amorphous layer surrounding the particles.

the carriers are predominantly electron-like, there are strong electron–electron correlations, and there is clear evidence for the formation of a spin density wave (SDW) gap in the undoped compound [9]. An upper limit for the electron carrier concentration of 1×10^{21} cm^{-3} is inferred from Hall data just above T_c. Encouraging for potential applications is that in this $T_c = 28.2$ K compound, the resistive transition in a field suggests that H_{c2} is remarkably high, ∼30 T. The coherence lengths [8] are short, ∼35 Å, but not as short as in high temperature superconductors (HTSs), so intergrain connectivity may not necessarily be disrupted.

Recently a new family of oxypnictides has been prepared by high pressure synthesis, $ReFeAsO_{1-\delta}$, without fluorine doping [10]. For Re = Nd, a dome-shaped phase diagram was found for T_c versus oxygen deficiency. Here we study the magnetic properties of the compound from that series with close to the highest T_c reported, $NdFeAsO_{0.85}$. The tunability of the superconductivity by oxygen deficiency in these materials strongly resembles the HTS oxide systems, and, as we show below, the electromagnetic connectivity of these materials also resembles the HTS case.

2. Experimental methods and structural characterization

$NdFeAsO_{0.85}$ was made by high pressure synthesis as described elsewhere [11]. In this paper we study a sintered bar of the material of dimensions 2.9 mm × 1.7 mm × 1 mm which was about 85% dense, weighing 35 mg, and also we flake off powdered material from the bar. The particles flaked off the bar are a range of powder conglomerates, the largest being of the order of 100 μm across. Such particles are polycrystalline (the grain size is of order of microns), but the crystallites within them are likely to be better-bonded mechanically, and so perhaps also electrically better-connected, than the weakest bonding within the sintered bar. The powder conglomerates and smaller powder particles are all rather plate-like. Scanning electron microscopy (SEM; LEO 1525) was used to analyse the morphology of the sintered body. The SEM sample was produced by scraping the sintered body, with the resulting powder being affixed to a stub using carbon tape. SEM images revealed that the sample does not consist of a single phase, and energy dispersive x-ray (EDX) analysis was used to identify the chemical composition of particles with different morphologies. The superconducting phase was generally found to adopt platelet morphology (figure 1(a)). The EDX results suggest that crystallites of the superconducting phase are compositionally homogeneous, at least within the limits of SEM-EDX analysis. Particles exhibiting a partially delaminated layer structure were identified as being neodymium oxide (figure 1(b)). These type of particles are likely to contribute to the large paramagnetic background seen on the magnetization curves. Transmission electron microscopy (TEM) images were obtained using an

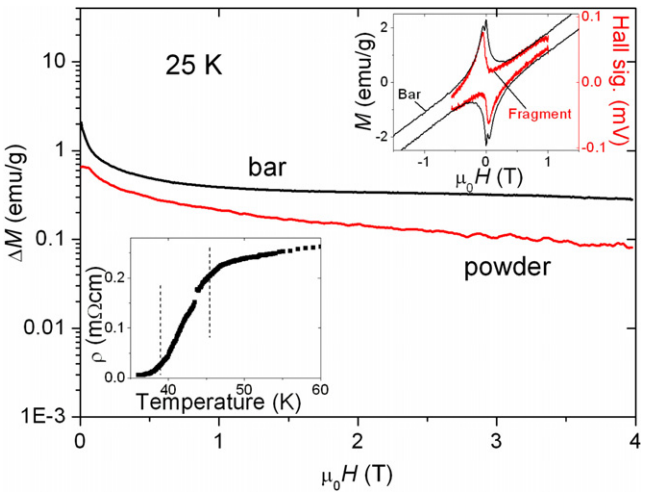

Figure 2. Irreversible magnetization versus magnetic field at 25 K on the powder and the bar sample. The top inset shows the bar M–H loop with the paramagnetic background measured with VSM and the fragment magnetic induction measured with the Hall sensor, both at 15 K. The bar and fragment loops show close agreement. The bottom inset shows resistivity versus temperature. The dashed lines mark the 10% and 90% points.

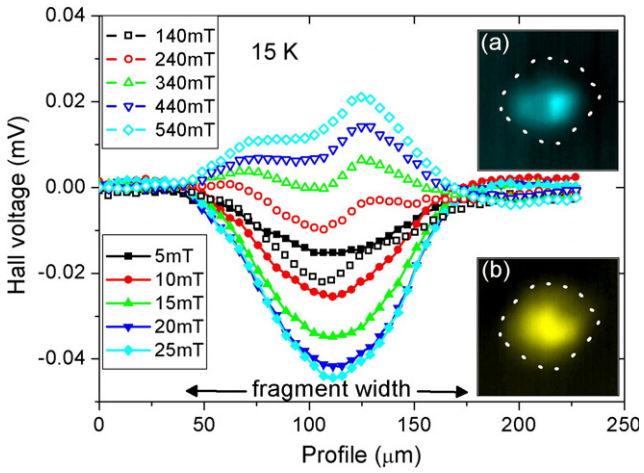

Figure 3. The cross-sections (B-$\mu_0 H$) taken from the Hall images at various applied magnetic fields on the 120 μm size fragment at 15 K on the virgin field-leg. Inset (a) shows the full image at 0.54 T (red (online) is positive M) and inset (b) shows the full image at 20 mT (yellow (online) is negative M). The dotted lines indicate the sample border.

FEI Titan operated at 300 kV. The powder scraped from the sintered bar was dropped on to a holey carbon coated copper grid. In the TEM observations, the majority of the electron-transparent samples exhibited the platelet morphology observed in the SEM. The platelets appear to consist of well-oriented layers and many have an amorphous phase that is 5–15 nm wide surrounding the particles (figures 1(c) and (d)).

Electrical transport measurements were made on the solid bar with dimensions 0.98 mm × 1.7 mm × 3.56 mm using a conventional four probe technique. An Oxford Instruments vibrating sample magnetometer with an 8 T superconducting magnet was used for magnetometry. Local Hall probe imaging was conducted using a scanning 5 μm InSb Hall cross micromagnetometer [12], and microcalorimetry was performed using a Si nitride membrane calorimeter, as described in detail elsewhere [13].

3. Results and discussion

Electrical transport data (see lower inset to figure 2) show that there are well-connected current paths through the whole bar. The main figure 2 shows that the irreversible magnetization Δm taken on the bar sample is larger than on the powder conglomerates at 25 K. Contributions to Δm from circulating currents depend on the length scale on which they flow [14]; there may be full connectivity, with currents circulating around the entire sample, or smaller regions of strong connectivity, or (as is often the case in HTS materials) poor intergranular connectivity, leaving only the intragranular currents to contribute. If we take the bar dimensions as the length scale for the global magnetometry, we can estimate a lower bound (if the currents flow, at least in part, on a smaller scale, the estimate for J_c is correspondingly higher) of $J_c = 10^3$ A cm^{-2}.

Figure 3 shows the results of Hall probe imaging of a single 120 μm conglomerate. The Hall images are approximately 200 μm across and reveal the magnetic intensity at a constant height 20 μm above the sample. The lower inset shows the magnetic image of the fragment at 15 K at 20 mT. In the images shown here, black represents zero local magnetization and bright regions represent areas of either positive local magnetization in the upper inset or negative local magnetization in the lower inset. At this temperature and field, the flux has a regular distribution, showing brightest regions (yellow online) with largest magnetization in the centre of the image. This is shown most clearly by a line-scan of the field image, which has a classic Bean profile (with some averaging because the sensor is ∼20 μm above the 120 μm size fragment) with partial penetration of flux at low field in agreement with the magneto-optical data of Prozorov *et al* [15]. The fragment only partially screens the field as would be expected from the geometry. Interestingly, the upper inset in figure 3 shows the same fragment at 15 K at 0.5 T where the magnetic response is dominated by a large paramagnetic background. (Note that regions of the fragment showing positive M are coloured cyan in the online version.) The upper inset to figure 2 shows the M–H loop and this large background signal is clear. Indeed the upper image shown in figure 3 shows a well-defined paramagnetic region particularly on the lower right-hand side of the sample. The profiles taken across the sample at 140 mT and above confirm the presence of the paramagnetic signal. Note that the paramagnetic material is distributed inhomogeneously, and is likely to be a second phase such as the Nd oxide imaged in figure 1(b). A weaker paramagnetic signal than we have seen here has recently been interpreted as an intrinsic property of Nd-based oxypnictides due to the existence of the magnetic Nd ions [16]. We believe that the inhomogeneity of the signal we see across the fragment, which is a good representation of the signal we see in the bulk (as shown by the upper inset to 2),

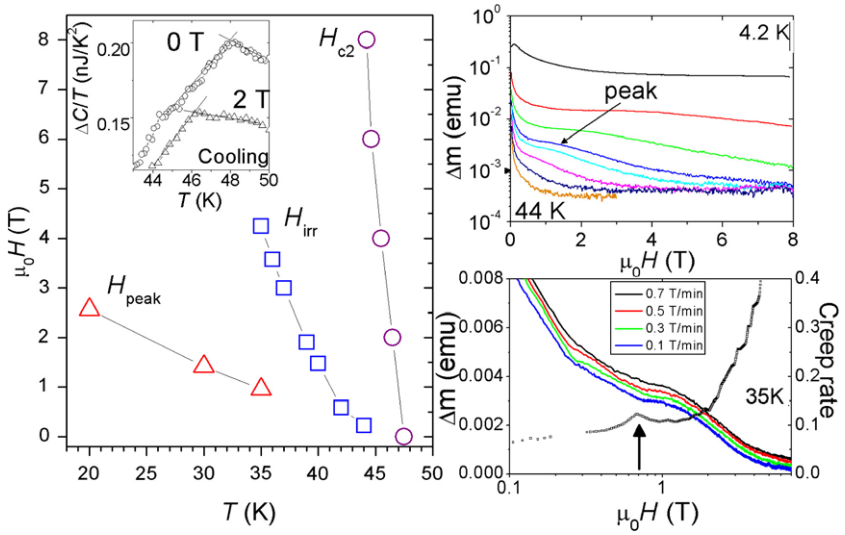

Figure 4. (Main) H–T diagram showing the irreversibility field $H_{\rm irr}(T)$ defined as the field at which the magnetic moment of the bar sample (32 mg) falls below 10^{-3} emu, the peak field $H_{\rm peak}$ versus temperature taken from the irreversible magnetization loops of the bar sample, and the upper critical field $H_{\rm c2}(T)$ taken from ac calorimetry measurements of the fragment. The inset to the main figure shows examples of the isofield measurements of heat capacity after subtraction of background (non-superconducting contribution) where ΔC is defined as $(C_{\rm total} - C_{\rm background})$. The top-right figure shows $\Delta m(H)$ (taken from the bar sample) for a range of temperatures (from top to bottom) 4.2, 20, 30, 35, 37, 40, 42, and 44 K. The bottom-right figure shows the normalized creep rate S (see text for definition) versus field at 35 K taken from the bar sample (black curve) and (left axis) associated $\Delta m(H)$ at 35 K for the different sweep rates 0.1, 0.2, 0.3, 0.5, and 0.7 T min^{-1}.

masks any underlying—presumably homogeneous—intrinsic paramagnetic signal in our samples.

From figures 2 and 3, using the Bean profile at full penetration (20 mT) and the magnetic signal above the single fragment (in the far field magnetic dipole limit) we can approximately estimate $J_{\rm c}$ in the single fragment to be of the order of 5×10^4 A cm^{-2} at 15 K. Again, this estimate is a lower bound, but probably a good one for the intergranular current density; there may well be a higher intragranular current density.

Figure 4 (main figure) plots the irreversibility line extracted from the irreversible magnetization of the bar sample (see figure 4 (top-right)) using a 10^{-3} emu threshold criterion. Note that the irreversible magnetization has a temperature-dependent, but field-independent, magnetic background which we subtract before estimating the $H_{\rm irr}$ threshold. To extract $H_{\rm c2}(T)$ we employed a microcalorimetry technique studying the same fragment imaged in figure 3. The heat capacity of the fragment was measured as a function of temperature in 0, 2, 4, 6, and 8 T as the system was cooled and warmed. To highlight the contribution due to the superconducting transition, the normal background heat capacity was estimated as a polynomial fit to the data and subtracted. The resultant peaks observed (inset to the main figure in figure 4) were used to determine the $H_{\rm c2}(T)$ curve plotted in the main figure [17]. To reduce error due to thermal gradient across the sample/gauge an average value was used for $H_{\rm c2}$, using the data taken when the sample was being cooled and warmed. Figure 4 also shows the position of the second magnetization peak $H_{\rm peak}$ determined as the maximum feature in $\mathrm{d}M/\mathrm{d}H$ at each temperature. The H–T diagram strongly resembles that of many of the highly anisotropic HTS systems [18].

We use the method known as 'sweep creep' [19], as first proposed by Pust *et al* [20], to determine the flux creep properties in this sample. We define the normalized dynamic creep rate, S, as $S = \mathrm{d}\ln\Delta M/\mathrm{d}\ln H'$, where H' is the sweep rate of the magnetic field, $H' = \mathrm{d}H/\mathrm{d}t$. By definition, S averages over two legs of the hysteresis loop, but permits rapid determination of the creep rate as a function of field. The bottom-right plot in figure 4 shows S and its variation with applied magnetic field in the bar at 35 K. There is clearly an approximate inverse relationship between the variation of $S(B)$ and $\Delta m(B)$. The first report of such a 'mirror image' relationship between the creep rate S and ΔM was made in HTSs in 1992 [21]. The flux creep observed in these oxypnictide samples is large, similar in magnitude to that in HTS materials, and the strong enhanced creep rate associated with the second peak feature is also very pronounced in this system. A detailed study of vortex regimes in the oxypnictide superconductors based on the dynamic creep rate [22] is beyond the scope of this present paper, but it is already clear that many of the issues as well as much of the interesting science are similar to those that arose with the cuprate materials.

4. Conclusions

Here we report on the connectivity issue in the new superconducting oxypnictide materials. We find that the macroscopic bar of the material appears to carry a finite $J_{\rm c}$ which is a positive for possible applications of the material. Fragments taken from the bar show $J_{\rm c}$ values at least an order of magnitude higher than this, and from TEM and SEM studies it seems that these fragments are conglomerates of several small crystallites. Consequently the intragrain $J_{\rm c}$ may

indeed be of the order of 10^5 A cm^{-2}, which is encouraging, although there are clearly connectivity issues that need to be surmounted. The vortex phenomenology strongly resembles that of the cuprate superconductors showing second peak features, enhanced creep rates, and an irreversibility line well below the upper critical field.

References

[1] Lebegue S 2007 *Phys. Rev.* B **75** 035110
[2] Singh D J and Du M H 2008 *Phys. Rev. Lett.* **100** 237003
[3] Mazin I I, Singh D J, Johannes M D and Du M H 2008 *Preprint* 0803.2740 [cond-mat]
[4] Kurmaev E Z, Wilks R G, Moewes A, Skorikov N A, Izyumov Yu A, Finkelstein L D, Li R H and Chen X H 2008 *Preprint* 0805.0668 [cond-mat]
[5] Eschrig H 2008 *Preprint* 0804.0186 [cond-mat]
[6] Lee P and Wen X G 2008 *Preprint* 0804.1739 [cond-mat]
[7] Li J and Wang Y 2008 *Chin. Phys. Lett.* **25** 2232
[8] Sefat A S, McGuire M A, Sales B C, Jin R, Howe J Y and Mandrus D 2008 *Preprint* 0803.2528 [cond-mat]
[9] McGuire M A, Christianson A D, Sefat A S, Jin R, Payzant E A, Sales B C, Christen D K and Mandrus D 2008 *Preprint* 0804.0796 [cond-mat]
[10] Ren Z A *et al* 2008 *Europhys. Lett.* **83** 17002
[11] Ren Z A *et al* 2008 *Chin. Phys. Lett* **25** 2215
[12] Perkins G K, Bugoslavsky Yu V, Qi X, MacManus-Driscoll J L and Caplin A D 2001 *IEEE Trans. Appl. Supercond.* **11** 3186
[13] Minakov A A, Roy S B, Bugoslavsky Y V and Cohen L F 2005 *Rev. Sci. Instrum.* **76** 043906
[14] Angadi M A, Caplin A D, Laverty J R, Shen Z X and Tonolo P 1991 *Physica* C **177** 479
Caplin A D, Angadi M A, Laverty J R and Deoliveira A L 1992 *Supercond. Sci. Technol.* **5** S161–4
[15] Prozorov R, Tillman M E, Mun E D and Canfield P C 2008 *Preprint* 0805.2783 [cond-mat]
[16] Tarantini C, Gurevich A, Larbalestier D C, Ren Z A, Dong X L, Lu W and Zhao Z X 2008 *Preprint* 0805.4445 [cond-mat]
[17] Senatore C, Wu G, Liu R H, Chen X H and Flükiger R 2008 *Preprint* 0805.2389 [cond-mat]
[18] Cohen L F and Jensen H 1997 *Rep. Prog. Phys.* **60** 1581
[19] Caplin A D, Cohen L F, Perkins G K and Zhukov A A 1994 *Supercond. Sci. Technol.* **7** 412–22 and the references therein
[20] Pust L, Kadlecova J, Jirsa M and Durcok S 1990 *J. Low Temp. Phys.* **78** 179
[21] Krusin-Elbaum L, Civale L, Vinokur V M and Holtzberg F 1992 *Phys. Rev. Lett.* **69** 2280
[22] Perkins G K, Cohen L F, Zhukov A A and Caplin A D 1995 *Phys. Rev.* **51** 8513–20